Lipid topology and electrostatic interactions underpin lytic activity of linear antimicrobial peptides in membranes.

David J. Paterson[a], Manlio Tassieri[a], Julien Reboud[a], Rab Wilson[a] and Jonathan M. Cooper[a,1].

Supplementary Information.

Materials and methods

Chemicals and reagents. All lipids were purchased from Avanti Polar Lipids (Avanti Polar Lipids, Alabama, USA) and used without further purification. 3 kDa dextran-AlexaFluor488 fluorescent dye was purchased from Molecular Probes (Life Technologies Ltd., Paisley, UK). Melittin and magainin 2 amide was obtained from Sigma-Aldrich (Sigma-Aldrich Company Ltd., Dorset, UK). Sylgard 184 PDMS monomer and curing agent were purchased from Dow Corning (Dow Corning, Massachusetts, USA).

Microfabrication. The device was manufactured as a PDMS cast from a silicon and SU8 master mold, as described in [23], using standard photolithographic techniques. A plan view of the device is shown in Fig. S1A.

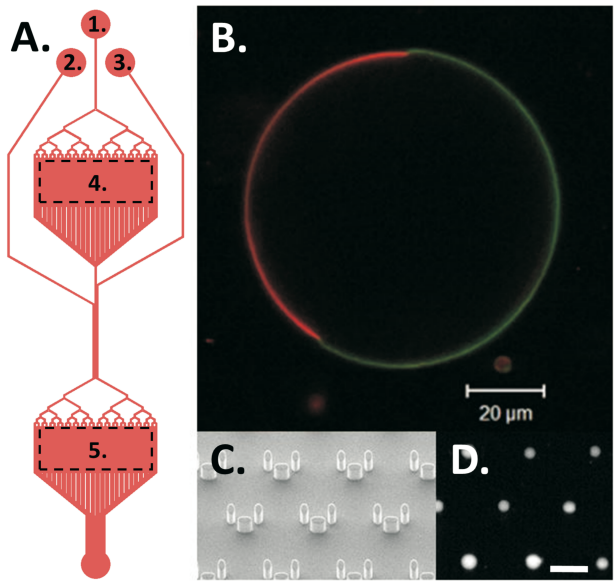

Fig. S1: (A) Plan view of the device, with the following parts labelled; 1) Flow channel; 2) Peptide channel; 3) Wash channel; 4) Electroformation chamber; 5) Microtrap array chamber. (B) A mammalian biomimetic GUV (system #A) with the liquid-disordered DOPC domain visualized with 0.1 mol% DPPE-rhodamine (red), and the liquid-ordered domain visualized using 0.5 mol% cholesterol-TopFluor (green). (C) SEM image of the microarray traps. (D) Vesicles trapped within the microarray, encapsulating 3 kDa dextran-AlexaFluor488. Scale bar = 100 µm.

Microtrap geometry was characterised by scanning electron microscopy, shown in Fig. S1C. The device was plasma bonded to the conductive surface of an indium tin oxide (ITO)-coated microscope slide, then incubated overnight at 4 °C in a 0.1 % BSA solution, coating the channels and microtrap arrays with BSA. The chip was then flushed with a 100 mM glucose, 5 mM HEPES (pH adjusted to 7.4 using 25% KOH) solution.

GUV electroformation. Vesicles were manufactured using modified versions of previously established protocols,[39][40] with lipid mixes of different charge and topographies, as described in Table S1.

Table S1. Membrane lipid compositions.

System	Lipid composition (60:40:40 mol %)	Melittin vesicles*	M2A vesicles*
#A	DOPC:DPPC:chol	121	354
#B	DOPC:DPPC:DOPG	86	76
#C	DOPC:DPPC:DPPG	71	59
#D	DOPC:DOPE:DOPG	167	34
#E	DOPC:DOPE:POPG	47	46
#F	DOPC:DOPE:DPPG	44	55
#G	DOPC:DOPE:LPG	138	35

DOPC: dioleoyl-phosphatidylcholine; DPPC: dipalmitoyl-phosphatidylcholine; chol: cholesterol; DPPG: dipalmitoyl-phosphoglycerol; DOPE: dioleoylphosphatidyl-ethanolamine; POPG: 1-palmitoyl-2-oleoyl-phosphoglycerol; LPG: lyso-phosphoglycerol. The third and fourth columns indicate the number of GUVs exposed to both melittin and m2a respectively. Total number of vesicles from at least three experimental runs.*

A 3.75 mg/ml solution of the desired lipids (60:40:40 mol %) in 95:5% chloroform:acetonitrile, was spin-coated at 400 rpm onto the conductive surface of an ITO-coated glass slide. The slide was dried under vacuum for 90 minutes, to remove all traces of organic solvent. The slide was then placed, lipid film side down, onto the PDMS device using a bespoke clamp, creating a central electroformation chamber. A solution of 100 mM sucrose, 5 mM HEPES (pH adjusted to 7.4 using 25 % KOH), 10 µM of 3 kDa dextran-AlexaFluor488 was injected into the central chamber. An AC-field sequence was then applied across the two slides, as shown in Table S2.

Table S2. Electoformation field parameters.

Frequency (Hz)	Voltage (Vpp)	Waveform	Duration (m)
10	0.1	Sine	10
10	0.5	Sine	20
10	1.0	Sine	30
10	1.6	Sine	120
3	2.0	Square	60

The AC electroformation pulse parameters for GUV production. The square wave field was applied in order to detach the GUVs from the slide. Electroformation for DPPC-containing GUVs (systems #A, #B and #D) carried out at 60 °C, above the transition temperature of DPPC, to ensure mixing of the lipid components. 0.05 mol% of DPPE-rhodamine was included within all lipid mixes, to enable fluorescent visualization of the vesicles.

Care was taken to osmotically match the interior sucrose and external glucose solutions using a micro-osmometer (Advanced Instruments, MA, USA) in order to avoid osmotic stress on the GUVs,. The vesicles produced were predominantly unilamellar (> 90%) and typically 10 to 30 µm in diameter. The mammalian biomimetic GUVs (system #A) displayed lateral phase separation between liquid-disordered DOPC and liquid-disordered DPPC domains (Fig. S1B). This phase separation replicates the *in-vivo* lipid rafts that exist in mammalian cell membranes.[18]

Experimental protocol. The device was loaded with vesicles as described in [23] and was washed using isosmotic solution from the flow channel, which resulted in a high density array of dye-loaded GUVs, gently pined against PDMS traps by microfluidic lamellar flow (shown in Fig. S1D). A 100 mM glucose, 5 mM HEPES (pH adjusted to 7.4 with KOH) solution doped with 1 μM of either m2a or melittin, was then flowed over the entrapped vesicles. The concentration of 1 μM is below the range of minimum inhibitory concentrations reported for both peptides, in various bacterial strains.[5][10][13] Due to the conditions of LCAMP binding within the microfluidic device, the use of a low concentration of peptide allowed helices to slowly accumulate within the vesicle outer leaflet, delaying the onset of LCAMP PIEs. The slow adsorption of peptides onto the GUVs membrane, allowed details regarding their activity to be revealed, which may have been obscured by faster peptide addition. Data for the 3 kDa dextran-AlexaFluor488, collected at a frequency of 0.25 Hz, using a Zeiss LDM 5 Live confocal microscope (Carl Zeiss Ltd., Cambridge, UK). All data presented within the paper is from a minimum of 3 experimental runs.

Data processing. The fluorescence intensity data was corrected for background fluorescence and photobleaching as shown in Fig. S2.

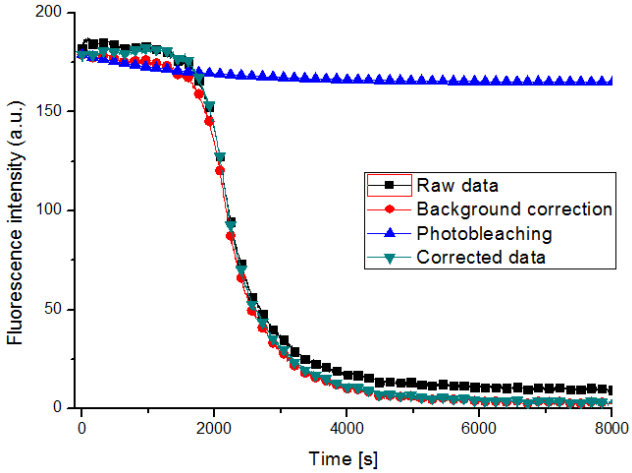

Fig. S2: Graph displaying the data processing to correct a 3 kDa dextran dye-leakage trace, for fluorescence background and photobleaching. Data collected from a DOPC vesicle, after exposure to 1 μM of the LCAMP melittin.. The data was then normalized, for a better comparison between different measurements.

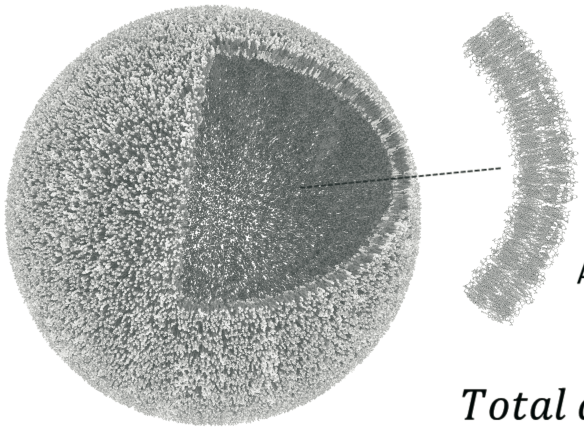

$$Flux = \frac{number\ of\ molecules}{area \times sec}$$

$$Area = A$$

$$Total\ amount\ lost = P\ x\ (C_{in} - C_{out}) \times A$$

Leakage timescale = τ:

$$\tau = \frac{number\ of\ molecules\ inside}{amount\ lost\ per\ second} = \frac{V \times Cin}{P \times A \times (Cin - C_{out})} = \frac{C_{in} \times \frac{4}{3}\pi r^3}{C_{in} \times P \times 4\pi r^2} = \frac{r}{3P}$$

Modelling a leak as a single exponential:

$$NFI = e^{-t/\tau} \Rightarrow -\ln(\mathrm{NFI}) = \frac{t}{\tau} \Rightarrow \frac{d}{dt}(-\ln(\mathrm{NFI})) = \frac{1}{\tau} = \frac{3P}{r}$$

Fig. S3: Calculations for the conversion of normalized fluorescence intensity (NFI), as a function of time, into the leakage timescale (τ) and the membranes apparent permeability. The calculations were performed via a dedicated LabView virtual instrument.

Analysis of pore-mediated leakage dynamics: Fig. S3 outlines the analytical method for determining the apparent permeability of a GUVs membrane, by monitoring the dye-efflux process. In particular, it is assumed that:

(i) The dye concentration inside (C_{in}) is homogeneous, since the time for a molecule of 3 kDa dextran, to diffuse a distance equal to an average GUV radius of r ~ 10 μm is ~2s, while the monitoring rate is 0.25s^{-1}.

(ii) The dye concentration outside (C_{out}) is equal to zero, due to the continuous flow washing away any leaked dye.

To analyse the normalised fluorescence intensity (NFI), it is assumed that the differential loss of dye from a GUV of volume V, equals the flux of dye through the membrane (of area A and apparent permeability P), occurring within the differential time dt. $-Vdc_{in} = PA(c_{in} - c_{out})dt \equiv PAc_{in}dt$. It follows that the leakage dynamics can be described (instant by instant) by a single exponential:

$NFI \propto c_{in} = \exp(-t/\tau)$, where $\tau = r/3P$ is the characteristic time of the process. In the case of multi-mode leakages, the above equation provides the opportunity to monitor the membranes apparent permeability during the changes in leakage dynamics, as shown in Fig. 3A to 3C, and schematically described in Fig. S3. The NFI curves were analysed, as described above, by means of a dedicated Labview (National Instruments) virtual instrument, which is available at DOI: 10.5525/gla.researchdata.434.

The membranes apparent permeability showed grouping into allowed flux rates, when compiled into histograms (see Fig. 3). A Shapiro-Wilks test was performed, which demonstrated that the data was not a random sampling of a normal distribution, to a high degree of confidence for all groupings ($P < 0.05$).

PIE Classification

LCAMP PIEs. Fig. S4 presents the PIEs reported in the literature for LCAMP activity.[6-9] For a vesicle to be categorized as belonging to a PIE, it had to meet the conditions given in the following sections, which describe the main forms of dye-efflux processes; e.g. pore-mediated leakage, a detergent-like carpet mechanism, and vesicle bursting.

No effect. GUVs can display no effect from peptide exposure over the experimental time course, defined as retaining 100% of the encapsulated dye, coupled to no loss in vesicle volume.

Pore-mediated leakage. The literature describes two forms of pore-mediated leakage; (i) graded, where vesicles lose a portion of their encapsulated dye and (ii) all-or-none, where vesicles lose 100% of their internal dye.[41] To be classified as a pore-mediated leakage event, a GUV had to lose at least some of its contents, with no accompanying loss of vesicle volume. We found that all pore-mediated leakage events occurred via the all-or-none mechanism (shown in Fig. S5).

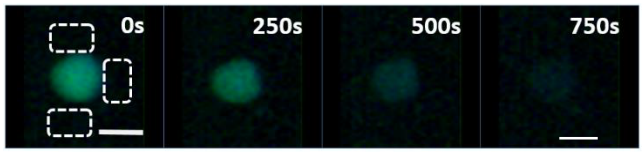

Fig. S5: Time series of a pore-mediated leakage event, occurring after exposure to 1 μM of the LCAMP m2a, within a system #C GUV. The event initiated after 200s. The scale bar represents 20 μm. Still images taken from Video S1.

Carpet mechanism. Gradual dye-efflux from a GUV, accompanied by a loss of vesicle volume, is characteristic of a carpet event, shown in Fig. S6. Carpet mechanism is associated with the ejection of tightly curved lipid-peptide micelles from the membrane, which are responsible for the loss in vesicle volume.

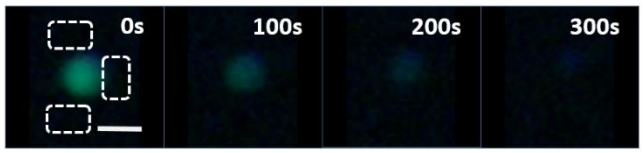

Fig. S6: Time series of a carpet mechanism leakage event, within a system #C, exposed to 1 μM of melittin. The event initiated after 2800s of exposure to peptide. The scale bar represents 20 μm. Still images taken from Video S2.

Bursting. Bursting events were classified as a total failure of a GUVs membrane, resulting in instant total loss of vesicle contents and volume, as shown in Fig. S7.

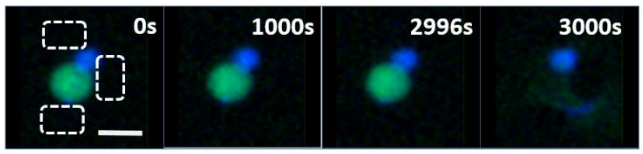

Fig. S7: Time series of a bursting event, occurring after exposure to 1 μM of m2a, within a system #F GUV. The event initiated after 168 s of exposure to peptide. The scale bar represents 20 μm. Still images taken from Video S3.

Other. A small proportion of vesicles (average ~ 3%) displayed PIEs that did not classify according to the criteria described above. Some GUVs underwent a micellisation, which we defined as an instantaneous loss of both encapsulated dye and vesicle volume. Unlike bursting, where the vesicle membrane totally failed, after a micellisation event, a new smaller vesicle remained. The authors have tentatively identified this event as the reformation of a vesicle after a bursting event.

Pre-pore regions. Membrane-bound LCAMPs helices form dynamic lipid-peptide rafts within the outer membrane leaflet, continually exchanging lipids with the bulk membrane. Each lipid contributes to the raft energy, through interactions with the peptides helical face, resulting in a heterogeneous population of rafts, having different E_L and γ. Lipids producing lower energy rafts (i.e. low σ_L and E_L) will be retained longer than those producing higher energy rafts.[27] Electrostatic interactions can force association between the cationic peptide and anionic lipids,[12] increasing the frequency of high energy rafts within the raft population. Lateral diffusion of the helices

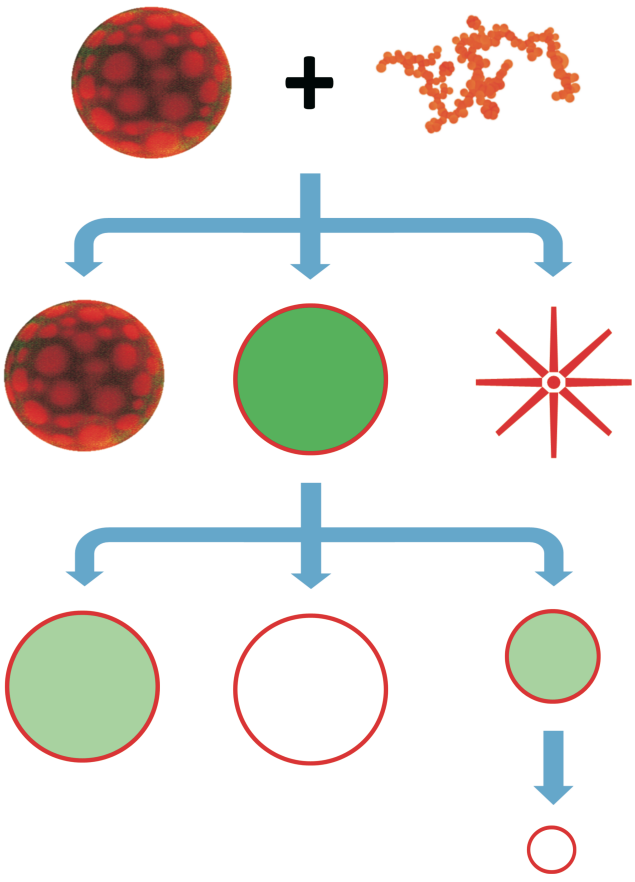

Fig. S4: Description of the PIEs recorded after vesicle exposure to the LCAMPs melittin and m2a, categorized as shown in Figs. S2 to S5. Vesicles can be left unchanged (no effect), burst, or exhibit dye-leakage via three mechanisms; gradient or all-or-none pore-mediated leakage, or a detergent-like carpet mechanism.

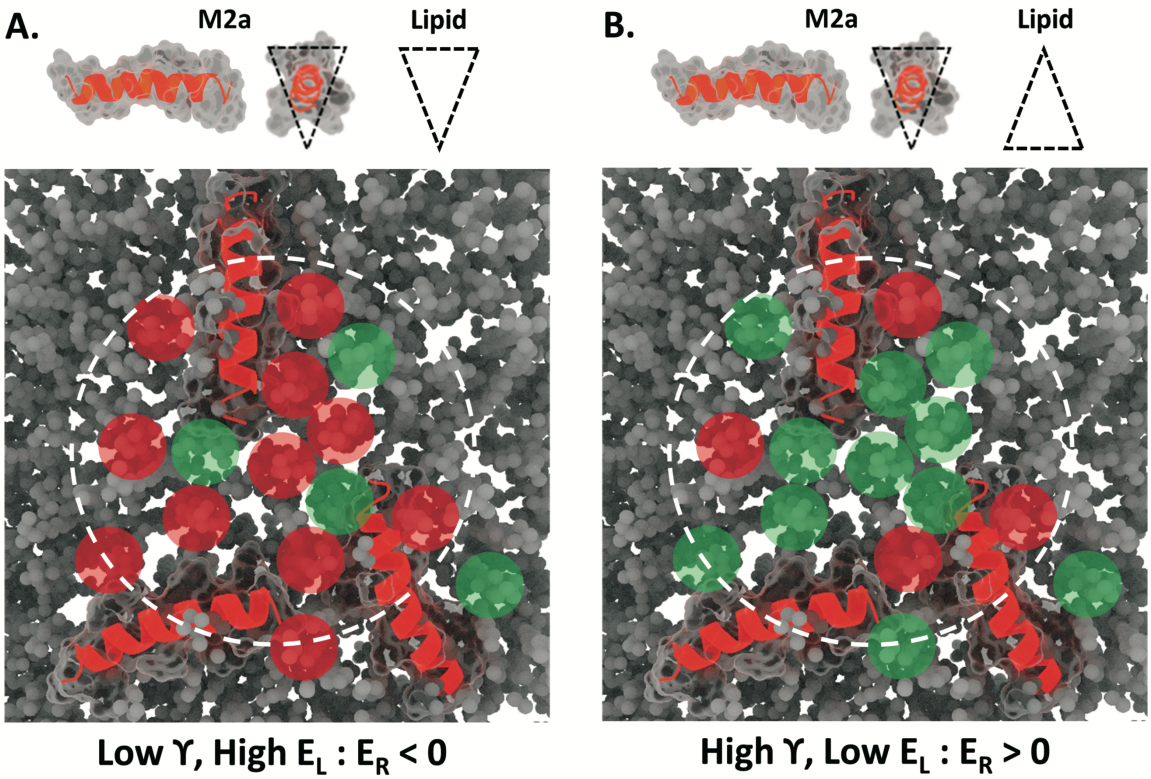

Fig. S8: The aggregation of LCAMP helices within a small pre-pore region, indicated by the dashed white line, can potentially accumulate significant membrane packing frustration (E_L) within a small region. (A) M2a helices surrounded by inverse-conical lipids, form high energy lipid-peptide interactions (red shading). Together with the efficient pore leaflet fold packing of inverse-conical lipids, this satisfies the conditions for pore formation; i.e. renders $E_R < 0$. (B) M2a surrounded by conical lipids generates low E_L (green shading). Conical lipids also increase γ, leaving the raft assembly unable to satisfy the conditions for pore formation.

creates transient raft assemblies as shown in Fig. S8, a membrane region with the potential to form a pore. To satisfy the thermodynamic conditions for pore formation the raft assembly must contain enough packing frustration that, when combined with the LCAMP-induced membrane thinning, it can overcome the integrity of the bilayer; i.e. render $E_R < 0$ as shown in Fig. S8A. High energy raft assemblies that do not satisfy the conditions for pore formation; e.g. rafts enriched with large hydrophobic volume lipids will react via other PIEs.

Hexagonal phase and leaflet fold packing. The leaflet-fold moiety of an idealized toroidal pore has a pronounced similarity with hexagonal phase packing structures, adopted by positive curvature lipids in aqueous environments.[35] Fig. S9 shows that both lipidic structures have tight positive curvature resulting from the bending of lipids from the headgroup towards the tailgroup. The pores' leaflet fold moiety bends the outer and inner membrane leaflets together, while hexagonal phase packing is formed of tightly curved lipid cylinders.

PIE initiation timings. The initiation times for the PIEs produced by m2a and melittin are presented in Table S3, and discussed in the Sections below, in the context of the topological model for LCAMP activity.

Pore initiation. Melittin induces fast pore formation in the membrane systems #A (DOPC:DPPC:cholesterol), #B (DOPC:DPPC:DOPG) and #D (DOPC:DOPE:DOPG), displaying average initiation times of 1614.8s, 450.6s and 1556.8s respectively. Large hydrophobic volume membrane components, i.e. DOPG and cholesterol, induce rapid, but not necessarily numerous, pore formation. In systems #A (37%)

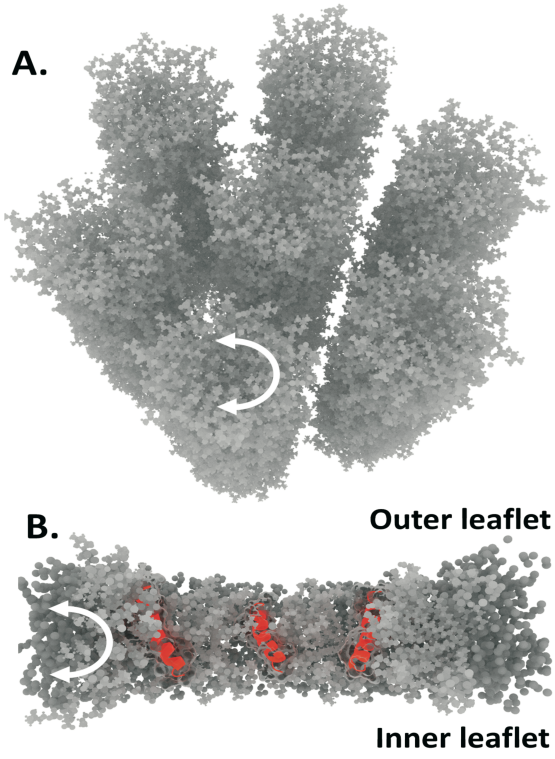

Fig. S9: Comparison between the laflet fold moiety of an idealised toroidal pore (A), and the hexagonal phase packing arrangement of inverse-conical lipids in aqueous environments (B). Both lipid packing arrangements involve tight positive curvature, bending the lipids from headgroup to tailgroup, shown by the white arrows.

Table S3A. Melittin PIE initiation timings.

Membrane system	Lipid composition	Vesicle size (μm +/- SD)	Pore initiation (s +/- SD)	Bursting initiation (s +/- SD)	Carpet initiation (s +/- SD)
#A	DOPC:DPPC:chol	25 +/- 9	1615 +/- 744	1125 +/- 723	1203 +/- 728
#B	DOPC:DPPC:DOPG	19 +/- 6	451 +/- 175	616 +/- 227	527 +/- 328
#C	DOPC:DPPC:DPPG	17 +/- 6	2541 +/- 1375	1418 +/- 879	2554 +/- 2921
#D	DOPC:DOPE:DOPG	19 +/- 8	1557 +/- 1217	1187 +/- 596	1650 +/- 1258
#E	DOPC:DOPE:POPG	12 +/- 7	4351 +/- 1672	4367 +/- 2244	N/A
#F	DOPC:DOPE:DPPG	12 +/- 5	4042 +/- 2575	3736 +/- 2596	258 +/- 232
#G	DOPC:DOPE:LPG	17 +/- 7	2223 +/- 1366	1795 +/- 2170	1812 +/- 1852

Table S3B. M2a PIE initiation timings.

Membrane system	Lipid composition	Vesicle size (μm +/- SD)	Pore initiation (s +/- SD)	Bursting initiation (s +/- SD)	Carpet initiation (s +/- SD)
#A	DOPC:DPPC:chol	20 +/- 7	3036 +/- 2427	2215 +/- 2149	2906 +/- 2204
#B	DOPC:DPPC:DOPG	19 +/- 8	1815 +/- 1087	1594 +/- 1939	N/A
#C	DOPC:DPPC:DPPG	25 +/- 8	3255 +/- 1620	N/A	1770 +/- 1657
#D	DOPC:DOPE:DOPG	16 +/- 6	N/A	N/A	N/A
#E	DOPC:DOPE:POPG	19 +/- 8	N/A	525 +/- 531	1242 +/- 1683
#F	DOPC:DOPE:DPPG	14 +/- 6	290 +/- 302	4407 +/- 2038	1808 +/- 2183
#G	DOPC:DOPE:LPG	20 +/- 8	3192 +/- 3033	1678 +/- 2438	188 +/- 60

Average PIE initiation times for the biomimetic lipid systems A to G, after exposure to 1 μM of the LCAMPs melittin (top) and m2a (bottom). The average initiation times for bursting, pore-mediated leakage and carpet mechanism are listed, together with their standard deviations, from at least three independent experiments.

and #B (58%) pore formation is both rapid and numerous, but system #D displays a lower event frequency of 17%. The discrepancy in pore frequency in these fast pore-forming membrane systems, can be explained within the framework of the topological model, through the consideration of the γ, σ_L and E_L values of the lipid-melittin rafts.

Lipid-melittin rafts enriched with DOPG and cholesterol possess high σ_G and E_L values, due to the synergy between lipid and peptide negative curvature topology, causing a high degree of packing frustration in the surrounding lipids. Raft assemblies of these high energy rafts can quickly overcome the cohesiveness of the bilayer, and induce quick PIEs. However, DOPG and cholesterol are inefficient packers of the pores rim, due to their high hydrophobic volume, increasing γ. In system #D, the helical face of melittin is enriched with DOPC, another lipid with high hydrophobic volume that will be inefficient at packing the pore. This creates a situation where a membrane-bound LCAMP helix forms high energy rafts, but cannot satisfy the conditions for pore-formation, due to a high γ. The lipid-peptide system will therefore react via another PIE, rather than pore formation; in the case of system #D, the carpet mechanism (47%) and bursting (33%) are preferred.

In systems #A and #B, the helical face of melittin will be enriched with the inverse-conical lipid DPPC, a positively curved lipid that is an efficient packer of the leaflet fold structure, giving low γ and enhanced pore formation. Systems #B and #D differ only by the substitution of 20 mol% of the lipids DPPC and DOPE. System #B (DPPC) demonstrates the second fastest initiation of pore formation of any lipid-peptide system tested, over threefold faster than system #D (DOPE). This demonstrates the sensitivity of melittin to zwitterionic lipid topology, due to the charge distribution of melittin leaving the helical face of the peptide free to interact with zwitterionic lipids.

Slowest pore formation for melittin occurred in systems #C (2541.0s), #E (4351.4 s) and #F (4041.7 s). These membranes all form lipid-melittin rafts enriched with inverse-conical anionic lipids; DPPG in system #C, POPG in system #E and DPPG in system #F. Although inverse-conical lipids lower the pore energy (γ) through leaflet fold stabilization, they also act in opposition to a key factor controlling melittin activity – the large increase in hydrophobic volume caused by deep penetration into the outer membrane leaflet. The resulting decrease in σ_G and E_L, means more melittin monomers must bind to the membrane, before sufficient membrane tension is achieved, leading to slower initiation of pore formation.

M2a demonstrates significant pore activity in the membrane systems #C (38%), #F (42%) and #G (14%), which return pore formation initiation times of 3255.4s, 289.5s and 3191.7s respectively. System #F (DOPC:DOPE:DPPG) demonstrates the quickest initiation of pore-mediated leakage events for any of the lipid-LCAMP systems tested., Within system #F membranes, m2a manipulates all three terms of the equation (γ, σ_G and E_L) and generates efficient pore formation. The electrostatically forced clustering of DPPG along the helical face of m2a lowers γ, and increases both σ_G and E_L. The positive curvature lipid DPPG stabilizes the pores leaflet fold structure, lowering the pore energy, and favoring pore formation. The synergy with the positive curvature induction of m2a will result in a larger increase in leaflet area asymmetry per peptide monomer that binds to the membrane, and generates a large amount of packing frustration around the membrane-bound

peptide (i.e. high E_L). σ_G will also be influenced by the presence of the non-bilayer lipid DOPE in the bulk membrane, which induces strain within bilayers,[31] and reduces the negative work needed to open the pore structure. E_L will be further increased by the steric crowding between the positive curvature anionic lipid DPPG, and the sterically bulky F residues of m2a, generating high energy lipid-m2a rafts. Together with the leaflet fold stabilization from the peptides three F residues, this combination of factors leads to rapid pore formation within system #F vesicles, quickly rendering $E_R < 0$, and favoring the formation of pores over other PIEs.

In a marked similarity with the melittin data set, exchanging 20 mol% of the lipids DOPE and DPPC alters the initiation of pore formation for m2a. However, in contrast to melittin, it is the replacement of DPPC with DOPE that speeds pore formation, rather than the converse. The selective m2a requires the non-bilayer lipid DOPE to weaken the membrane, but can stabilize the pore leaflet fold structure due to its three phenylalanine residues. The non-selective melittin destabilizes the membrane through its deeper penetration into the outer leaflet, but as the peptide contains only one tryptophan residues, i.e. it lacks the positive curvature stabilization of m2a, and requires the presence of the inverse-conical DPPC to generate low γ. The requirement for the presence of DOPE or DPPC to initiate the quickest pore formation is therefore reversed between the peptides; i.e. M2a requires DOPE to weaken the membrane, while melittin requires DPPC to form stable pore leaflet fold structures.

It is interesting to note that both melittin and m2a are capable of rapid pore formation in the membrane systems containing lipids characteristic of their intended targets; mammalian membranes are primarily composed of bilayer lipids like DPPC,[18] while bacterial membranes typical contain conical non-bilayer lipids lipid DOPE.[19] M2a is tuned by the relationship between its topological and charge properties, and the lipid-peptide interactions with its membrane-bound helix, to be selective for bacterial cells. It operates in the narrow gap between the lamellar to non-lamellar phase transition seen in bacterial membranes, compared to mammalian membranes.[27] M2a requires a more unstable membrane to initiate pore formation, but under optimal conditions forms rapid pores.

Carpet mechanism initiation. Systems #C (DOPC:DOPE:DPPG) demonstrates the fastest initiation of the carpet mechanism PIE (258.3 s) when exposed to melittin, but the event is a low frequency occurrence (10 %), suggesting that it may be caused by relatively rare lipid-peptide interactions; e.g. the association of high energy but low frequency lipid-melittin rafts featuring DOPE. Melittin in conjunction with DOPE accumulates negative curvature within the membrane, stabilizing the formation of the tightly curved micellular structures which are expelled from the membrane during carpet mechanism events. The membranes that generate the next two fastest initiation times for the carpet mechanism are the mammalian biomimetic membrane system #A (1202.5 s) and bacterial biomimetic membrane system #B (526.9 s), with both returning > 30 % event frequencies for the carpet mechanism. Both systems also feature a negative curvature membrane component that can be expected to become enriched within the lipid-melittin rafts. System #A contains cholesterol, which will preferentially associate with the peptide through aromatic π-stacking interactions with melittin's tryptophan residue;[28][29] system #B contains the anionic lipid DOPG, which will associate through electrostatic interactions with the cluster of cationic residues at the peptides c-terminus.[12]

Conversely, m2a demonstrates faster carpet mechanism events within membrane systems containing positively curved anionic lipids; systems #E (DPPG) and #G (LPG) returning initiation times of 1241.7 s and 187.5 s respectively. The rapid nature of carpet mechanism initiation in system #G is particularly worthy of comment, being the fastest initiation of any PIE within any membrane system, for either of the peptides. The association via electrostatics, of the cationic positively curved m2a and the anionic highly positively curved LPG ($S < 1/3$), concentrates a large amount of positive curvature within the membrane: enough to stabilize the highly curved lipid peptide micelles generated by the carpet mechanism. Membrane systems containing anionic lipids with larger hydrophobic volumes (i.e. DOPG in systems #B and #D), generate no carpet events, suggesting clustering with unsaturated 18:1 (9Z) hydrocarbons is sufficient to suppress the carpet activity of m2a. The mammalian biomimetic GUV system #A (DOPC:DPPC:cholesterol) generates the slowest carpet mechanism events, through the enrichment of the lipid-m2a rafts with cholesterol. The presence of the negative curvature lipid cholesterol will counteract the positive curvature induction of m2a, preventing the accumulation of the curvature required to form micellular structures

Image production: The lipid and peptide rendered figures were assembled using two 3D modelling and lipid simulation tools: Lipidwrapper, an algorithm developed by Jacob Durrant, at the University of California;[42] CHARMM, a program for the generation of molecular dynamics simulation models, developed by the research group of Professor Martin Karplus at Harvard University.[43][44] Pymol, an open source molecular visualization system, was used to generate the peptide models directly from Protein Data Bank (.pdb) files. Lipids and peptides were then assembled within Blender, an open source 3D creation suite, and then rendered.